NANO LETTERS

pubs.acs.org/NanoLett

Microstructure and Pseudocapacitive Properties of Electrodes Constructed of Oriented NiO-TiO_2 Nanotube Arrays

Jae-Hun Kim, Kai Zhu,* Yanfa Yan, Craig L. Perkins, and Arthur J. Frank*

National Renewable Energy Laboratory, Golden, Colorado 80401-3393, United States

ABSTRACT We report on the synthesis and electrochemical properties of oriented NiO-TiO_2 nanotube (NT) arrays as electrodes for supercapacitors. The morphology of the films prepared by electrochemically anodizing Ni−Ti alloy foils was characterized by scanning and transmission electron microscopies, X-ray diffraction, and photoelectron spectroscopies. The morphology, crystal structure, and composition of the NT films were found to depend on the preparation conditions (anodization voltage and postgrowth annealing temperature). Annealing the as-grown NT arrays to a temperature of 600 °C transformed them from an amorphous phase to a mixture of crystalline rock salt NiO and rutile TiO_2. Changes in the morphology and crystal structure strongly influenced the electrochemical properties of the NT electrodes. Electrodes composed of NT films annealed at 600 °C displayed pseudocapacitor (redox-capacitor) behavior, including rapid charge/discharge kinetics and stable long-term cycling performance. At similar film thicknesses and surface areas, the NT-based electrodes showed a higher rate capability than the randomly packed nanoparticle-based electrodes. Even at the highest scan rate (500 mV/s), the capacitance of the NT electrodes was not much smaller (within 12%) than the capacitance measured at the slowest scan rate (5 mV/s). The faster charge/discharge kinetics of NT electrodes at high scan rates is attributed to the more ordered NT film architecture, which is expected to facilitate electron and ion transport during the charge−discharge reactions.

KEYWORDS Supercapacitor, nickel oxide, nanotube, anodization

One-dimensional (1D) nanostructured materials (e.g., nanotube (NT) and nanowire arrays) have attracted recent attention for various applications, such as solar energy conversion,[1−9] electrochromic devices,[10,11] and electrochemical energy storage.[12−16] Electrochemical capacitors (also called supercapacitors or ultracapacitors) represent an emerging energy storage technology that offers high power density, long cycle life, short charging time, good safety, and so forth.[17−22] Supercapacitors can be used either alone as a primary power source or as an auxiliary power source with rechargeable batteries for high power applications, such as load cranes and hybrid/electric vehicles. Electrodes constructed from oriented NT arrays, aligned perpendicular to the current collectors, can readily be prepared with large surface areas, high packing densities, and ordered pore networks. These morphological properties are expected to facilitate rapid charge/discharge kinetics (high power density).[12−16] Moreover, because the NTs are in direct contact with the current collector, it may not be necessary to use conducting additives and binders, which would reduce both the weight and volume of the electrodes.

Supercapacitors can be classified by their reaction mechanisms into two categories. The first category is electrical double-layer capacitors (EDLCs), which are based on nonfaradic charge separation at the electrode/electrolyte interface. Carbon materials with high specific surface areas are usually used in EDLC electrodes.[17,18,21] The second one is pseudocapacitors (or redox-capacitors), which are based on the fast and reversible redox reactions at/near the surface of active materials (e.g., conducting polymers and metal oxides).[17,18,21] Pseudocapacitors generally show relatively less cycling stability than EDLCs because of the faradic reaction mechanism. However, pseudocapacitor electrodes show promise in asymmetric and/or hybrid configurations owing to their high specific capacitances (F/g) and high volumetric capacitances (F/cm^3) as a result of the densely packed active materials. Among various pseudocapacitor electrode materials, hydrous RuO_2 exhibits the most promising performance to date.[23−25] However, the high cost of RuO_2 has limited its commercial attractiveness for supercapacitor applications. Therefore, there has been extensive interest in developing alternative pseudocapacitor electrode materials, such as manganese oxide,[26−28] cobalt oxide,[29,30] and nickel oxide.[31−41]

In this paper, we examine the morphological and electrochemical properties of oriented NiO-TiO_2 NT arrays as pseudocapacitor electrodes. The arrays were fabricated by electrochemically anodizing Ni−Ti alloy foils followed by thermal annealing. The preparation of TiO_2 NT arrays by the electrochemical anodization of Ti was reported sometime ago.[42,43] However, unlike the anodization of Ti films in the commonly used fluoride-containing electrolytes to form NT arrays,[44,45] anodizing Ni films in similar electrolytes do not

* To whom correspondence should be addressed. E-mail: (K.Z.) Kai.Zhu@nrel.gov; (A.J.F.) AFrank@nrel.gov.

Received for review: 06/22/2010
Published on Web: 09/28/2010

DOI: 10.1021/nl102203s | *Nano Lett.* **2010,** *10,* 4099–4104

lead to the formation of NTs. Consequently, we investigated whether the Ti component in the Ni−Ti alloy foils could be used as a supporting material to form the NT structure.[46−48] The morphology, crystal structure, and composition of the NiO-TiO_2 arrays were found to depend on the anodization voltage and postgrowth annealing temperature. These structural changes were shown to have a strong influence on the electrochemical properties of the NiO-TiO_2 NT electrodes. Significantly, the NiO-TiO_2 electrodes exhibited rapid charge/discharge kinetics and long-term cycling stability, which are important properties for supercapacitors.

NiO-TiO_2 NT arrays were prepared by electrochemically anodizing Ni−Ti binary alloy foils (56 wt % of Ni, Alfa Aesar) in ethylene glycol solution, which contained 0.25 wt % NH_4F and 1.5 wt % H_2O; the counter electrode was a Pt mesh. The Ni−Ti foils were biased at 20, 40, 60, and 80 V for 5−10 min at room temperature. Anodizing Ni−Ti foils for longer periods did not produce thicker films, presumably because of equilibration between oxide forming and dissolving processes. Such phenomenon has been observed when Ti foils are anodized to form TiO_2 NT arrays.[49,50] The resulting Ni−Ti films were annealed for 1 h in air at temperatures ranging from 400 to 700 °C (ramp rate 5 °C/min). NiO nanoparticles were purchased from Aldrich (99.8%, < 50 nm, specific surface area of >50 m^2/g by BET). Films of the NiO nanoparticles were prepared by a similar procedure described for preparing TiO_2 nanoparticle films.[51] Briefly, a single-layered NiO film was applied from an organic paste (18.2 wt % NiO, 9.1 wt % ethyl cellulose, 72.7 wt % terpineol) via the doctor blade technique, and then it was annealed at a temperature of 600 °C. The average thickness of the NiO nanoparticle films was about 400 nm as measured with a surface profiler (KLA Tencor Alpha-Step 500). The crystal structures of the NT films were characterized by X-ray diffraction (XRD, SCINTAG DMS-2000 diffractometer with Cu K_α radiation, glancing angle mode). The morphology and microstructure of the films were examined by field emission scanning electron microscopy (FE-SEM, JEOL JSM-7000F) and high-resolution transmission electron microscopy (HR-TEM, FEI Tecnai F-20UT, operating at 200 kV) with energy dispersive X-ray spectroscopy (EDS). X-ray photoelectron spectroscopy (XPS, Physical Electronics PHI 5600 with monochromatic Al K_α radiation) was used for determining the composition of NTs and the chemical/oxidation state of Ni in the NT films. The binding energy scale of the spectrometer was calibrated using the well-known binding energies of the Cu $2p_{3/2}$, Cu L_3MM, and Cu $3p_{3/2}$ transitions found for clean polycrystalline foil. Low-energy resolution experiments were conducted with a 185 eV pass energy; higher resolution data were acquired with a 29.35 eV pass energy. All electrochemical measurements were performed with a three-electrode glass cell setup, which consisted of a NT working electrode, a platinum mesh counter electrode, and a Ag/AgCl reference electrode. Galvanostatic charge/discharge cycling and cyclic voltammetry (CV) of the electrodes in 1 M KOH solution were performed at room temperature with a potentiostat/galvanostat (VMC-4, Princeton Applied Research) at potentials between 0.0 and 0.5 V. The capacitances of the electrodes were calculated using the expression $I \times \Delta t/\Delta V$, where I is the constant discharging current, Δt is the discharging time, and ΔV is the voltage window (0.5 V) for the galvanostatic measurement. For CV curves, the capacitance was obtained from the integrated voltammetric charges divided by the same voltage window.

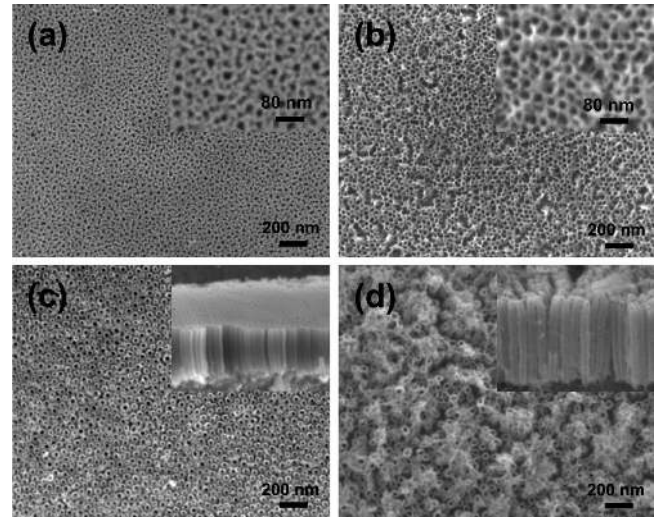

FIGURE 1. Surface and cross-sectional SEM images of as-deposited films that were prepared by anodizing Ni−Ti alloy foils at (a) 20, (b) 40, (c) 60, and (d) 80 V.

Materials Characterization. Figure 1 shows the SEM images of the as-grown films that were prepared by anodizing Ni−Ti foils at potentials of 20 (Figure 1a), 40 (Figure 1b), 60 (Figure 1c), and 80 V (Figure 1d). When the Ni−Ti foil is anodized at 20 V, the resulting film (Figure 1a) displays a nanoporous structure with irregular shaped pores. When the Ni−Ti foil is anodized at 40 V (Figure 1b), the pores of the resulting film become more regular; however, there are no distinct NT structures (Figure 1b inset). When the anodization voltage is increased to 60 V, the resulting film (Figure 1c) exhibits the expected NT array structure in which individual NTs are packed in approximately hexagonal symmetry. Analysis of the SEM images in Figure 1c shows that the average NT pore diameter, wall thickness, and intertube spacing are 38, 13, and 5 nm, respectively. From these parameters, we estimate[1] that the respective film porosity and roughness factor are 49% and 77 μm^{-1}. Cross-sectional SEM images (inset) indicate that the NT lengths range from 200 to 500 nm. When the anodization voltage is further increased to 80 V, the top surface of the NT film appears partially damaged owing to a rapid chemical dissolution reaction. However, the NT architecture is retained. Because of their well-defined architecture, the foils anodized at 60 V (Figure 1c) were used for the subsequent studies described in this paper.

DOI: 10.1021/nl102203s | *Nano Lett.* **2010,** *10,* 4099–4104

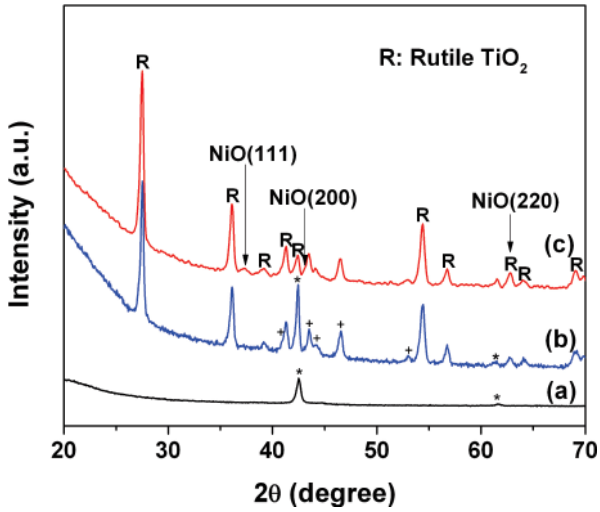

FIGURE 2. XRD patterns of the (a) as-grown NT film, (b) Ni−Ti foil annealed at 600 °C, and (c) NT film annealed at 600 °C. The peaks indicated by asterisks and crosses correspond to the NiTi and Ni_3Ti phases from the Ni−Ti foil, respectively.

Figure 2 shows the XRD patterns of the as-grown NT films before and after they were annealed at 600 °C. The XRD pattern of the Ni−Ti foil annealed at 600 °C is shown as a reference. It is worth noting that of the NT films annealed at temperatures between 400 and 700 °C, only those annealed at 600 °C displayed significant pseudocapacitive behavior (Figure 4). The characteristic peaks of rock salt NiO (e.g., $2\theta = 37.3°$) and rutile TiO_2 (e.g., $2\theta = 27.5°$) can be observed in the XRD patterns of the annealed NT film. In contrast, the as-grown NT film shows no diffraction peaks for the rock salt NiO and rutile TiO_2 phases. A comparison of XRD patterns of the NT arrays annealed at 400−700 °C is given in the Supporting Information (Figure S6). XPS measurements (see Figure S1 in the Supporting Information) indicate that a $NiTiO_3$-like phase might be present at the surface. However, this phase is not observed in either the XRD pattern or the selected area electron diffraction (SAED) pattern (see Figure S2 in the Supporting Information). These results suggest that annealing transforms the as-grown NT films from an amorphous phase to primarily a mixture of crystalline NiO and TiO_2.

The SEM image (Figure 3a) shows that the NT film architecture is preserved when a film was annealed at a temperature of 600 °C. The TEM image (Figure 3b) indicates that the structure integrity of the annealed NT walls is also maintained. The HR-TEM image (Figure 3c) shows that the NTs are polycrystalline with domains of different crystallite or grain sizes. For instance, regions R1 and R2 in Figure 3c show that the grain size of domain R1 is much larger than that of R2. Figure 3d,e shows the EDS spectra of R1 and R2, respectively. The circles in Figure 3c indicate roughly the size of the electron beam used for the EDS spectra. The EDS spectra reveal that the R1 and R2 crystalline domains correspond primarily to TiO_2 and NiO, respectively. The relatively strong Ti peaks observed in Figure 3e is consistent with a small NiO grain (R2) that likely overlaps with a TiO_2 grain. The carbon peak (C) in Figure 3e is due to surface contamination caused by the fine electron beam. Taken together, the results of Figures 2 and 3c−e suggest that the annealed NTs mainly consist of a mixture of crystalline domains of rutile TiO_2 and rock salt NiO phases.

Electrochemical Characterization. Figure 4 displays the cyclic voltammograms (CV) of as-grown and annealed NT films measured at a scan rate of 20 mV/s. The CV curves of the as-grown and 400 °C annealed NT films have approximately rectangular shapes, which are characteristics of electric double-layer capacitors. The inset of Figure 4 shows a pair of anodic and cathodic peaks at 0.43 and 0.36 V (vs Ag/AgCl), respectively, for a film annealed at 500 °C. This feature is not present in the cyclic voltammograms of the pure TiO_2 NT films measured under the same conditions; the cyclic voltammograms of TiO_2 NT electrodes display just a rectangular shape (data not shown). On the basis of the XRD results, we attribute the two peaks to the nickel oxide component in the NT films. Studies[34−37] of NiO electrodes indicate that the CV peaks are associated with the pseudocapacitive behavior resulting from the faradic oxidation and reduction reactions.[32−40]

$$NiO + OH^- \leftrightarrow NiOOH + e^- \quad (1)$$

For electrodes with films annealed at 600 °C, the peak current intensities, corresponding to the redox reactions, increase by a factor of 30, from about 0.01 mA/cm^2 at 500 °C to 0.3 mA/cm^2 at 600 °C. The sharp increase of the peak current density suggests that an annealing temperature of 600 °C is required to obtain a suitable NiO phase in the Ni−Ti−O NT arrays for the redox reactions to occur. In comparison to the NiO-TiO_2 NT electrodes, the Ni−Ti substrates annealed at 600 °C exhibit negligible charging/discharging current densities (see Figure S3 in the Supporting Information), indicating that the observed CV response is from the NiO-TiO_2 NTs. However, for electrodes with films annealed at 700 °C, the peak current intensities for both the anodic and cathodic reactions are reduced by 6-fold. The smaller peak current intensities are attributed to the collapse of the NT pore structure at 700 °C (see Figure S4 in the Supporting Information).

Figure 5a shows the cyclic voltammograms of a 600 °C annealed NiO-TiO_2 NT electrode at scan rates between 5 and 500 mV/s. Over the entire range of scan rates, the pair of cathodic and anodic peak curves are symmetrical, implying good reversibility of the redox reactions at/near the NT surfaces. The peak current intensity increases linearly with the scan rate (see Figure S5 in the Supporting Information), confirming the pseudocapacitive behavior of the NiO-TiO_2 NT electrode associated with NiO component. The linear increase of the current density response with the scan rate also indicates that the kinetics of interfacial faradic redox

DOI: 10.1021/nl102203s | *Nano Lett.* **2010,** *10,* 4099–4104

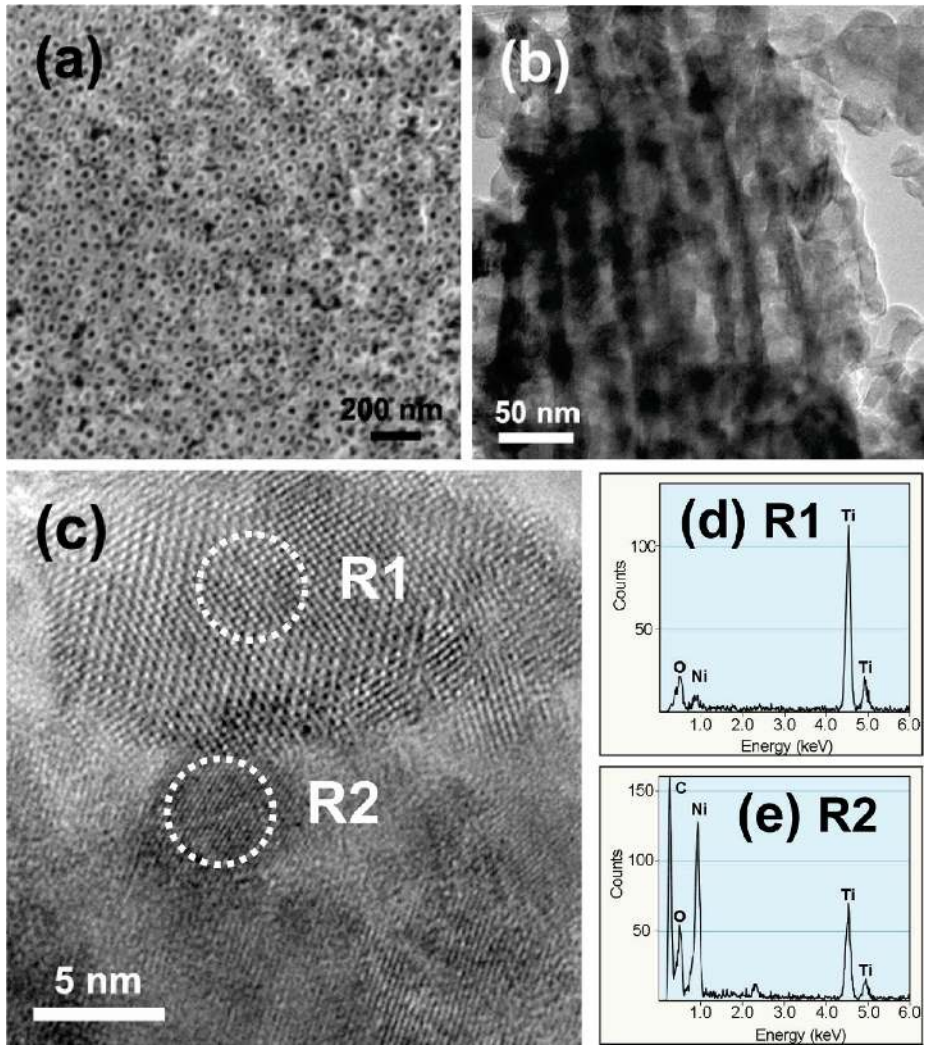

FIGURE 3. (a) SEM, (b) TEM, (c) HR-TEM images, and EDS spectra of (d) Region 1 (R1) and (e) Region 2 (R2) of the NT films annealed at 600 °C.

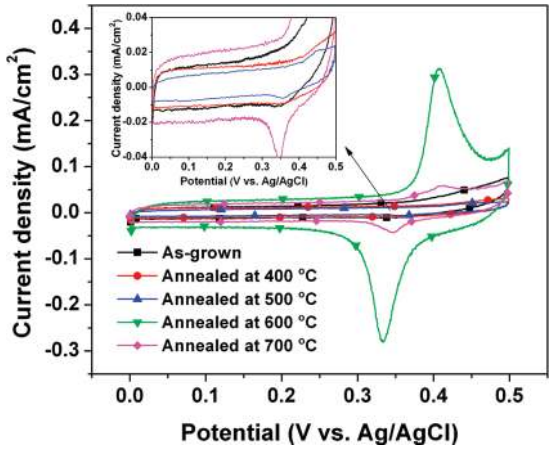

FIGURE 4. Cyclic voltammograms of the as-grown and annealed NT arrays. The annealing temperature ranges from 400 to 700 °C. The potential was scanned at a rate of 20 mV/s.

reactions and the rates of electronic and ionic transport are even rapid enough at scan rates as high as 500 mV/s. Figure 5b shows the rate dependence of the capacitance of the NT electrode used in Figure 5a. The rate capability of a NiO nanoparticle film with a similar film thickness and surface area as the NT electrode is also plotted in Figure 5b for comparison. The NT electrode exhibits a higher rate capability than the nanoparticle electrode. Moreover, at the highest scan rate (500 mV/s), the capacitance of the NT electrode is maintained up to 88 % of that measured at the scan rate of 5 mV/s. The faster charge/discharge kinetics of NT electrodes at high scan rates is attributed to the ordered NT film architecture. Presumably, the direct conducting pathways for electrons in the NT walls and for ions through the pore system facilitate the electronic and ionic transport during the charge−discharge reactions.

Figure 6a shows several cycles of representative voltage profiles of the NiO-TiO_2 NT electrodes from galvanostatic charge/discharge measurements performed at a constant current density (0.4 mA/cm^2). Figure 6b shows the cycling performance of the NiO-TiO_2 NT electrode for the first 500

DOI: 10.1021/nl102203s | Nano Lett. 2010, 10, 4099–4104

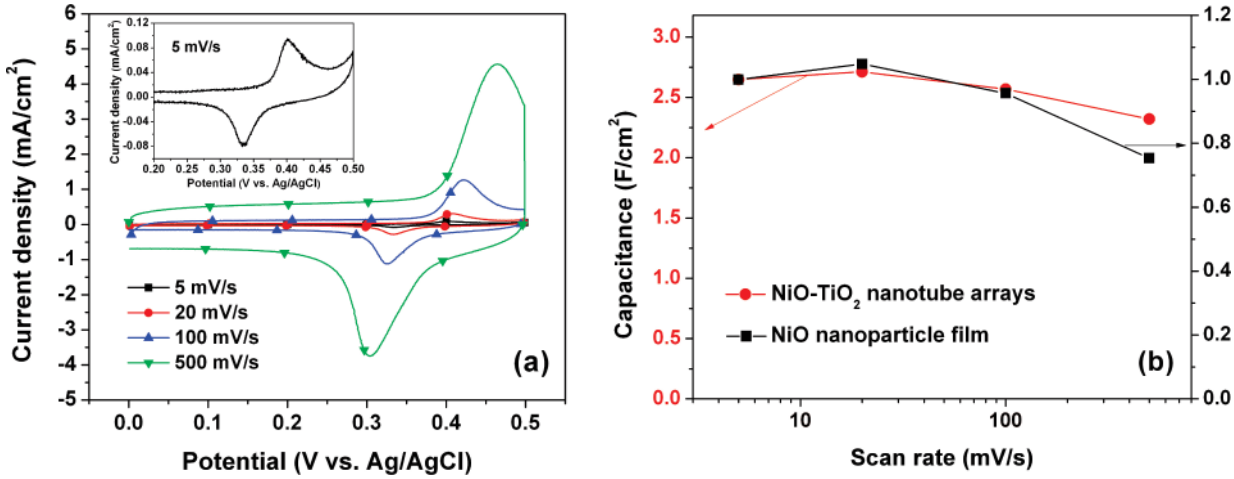

FIGURE 5. (a) Cyclic voltammograms of a 600 °C annealed NT electrode measured at scan rates from 5−500 mV/s. (b) Capacitance of the NT and nanoparticle electrodes plotted as a function of the scan rate.

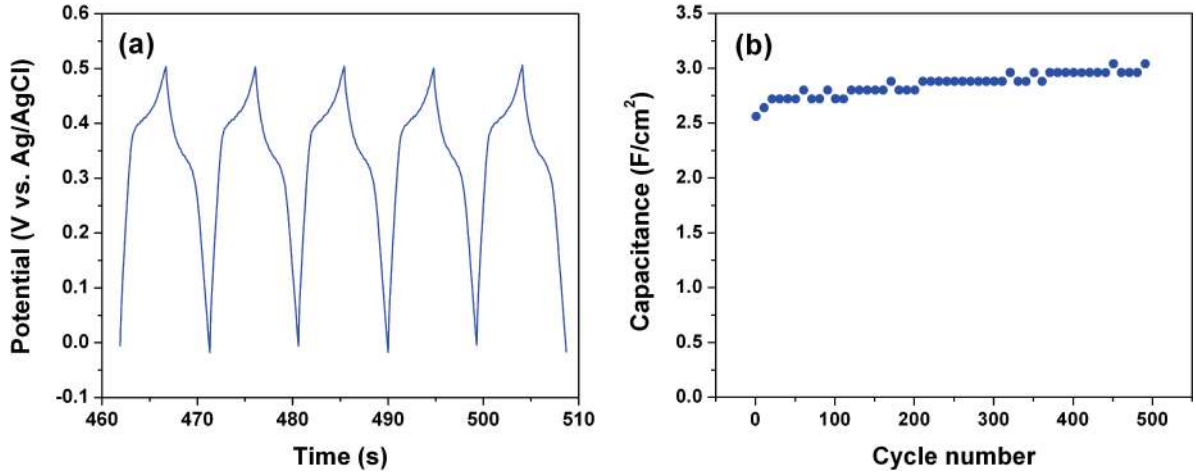

FIGURE 6. (a) Typical voltage profiles and (b) cycle performance of an electrode with a NT film annealed at 600 °C. The current density was held constant at 0.4 mA/cm^2.

cycles. The NT electrodes display stable long-term cycling performance, which is a requirement for supercapacitors. The weight of the NT films was estimated from the structural parameters of the films. From the film thicknesses (200−500 nm) and porosities (49%), we estimate that the specific capacitance of the NiO-TiO$_2$ NT electrodes were in the range of 40−100 F/g. Taking into account the Ni−Ti ratio of 1:2 determined from the EDS data (not shown), the specific capacitance of the NiO component of the NiO-TiO$_2$ NT films ranged from 120−300 F/g. It is expected that further increase in the specific capacitance can be obtained by optimizing the NiO-TiO$_2$ NT morphology (e.g., pore size, wall thickness, composition, and crystallinity).

In summary, it was demonstrated that the electrochemical anodization of Ni−Ti alloy foils at specific voltages followed by thermal annealing produces NiO-TiO$_2$ nanotube (NT) arrays. Variations in the preparation conditions (e.g., anodization voltage and thermal annealing temperature) change the morphology and crystal structure of the films, which, in turn, have a strong influence on the electrochemical properties of the electrodes. The electrodes composed of NiO-TiO$_2$ NT films annealed at 600 °C exhibit rapid charge/discharge kinetics and high stability during long-term cycling, which would be important for use as pseudocapacitors (redox-capacitors). The NT-based electrode displays a higher rate capability than the randomly packed nanoparticle-based electrode, which is attributed to the more ordered NT film architecture. Optimizing NT morphology (e.g., composition, crystallinity, surface area, and film thickness) is likely to further enhance the electrochemical properties of NiO-TiO$_2$ NT arrays as electrodes for supercapacitors. The knowledge gained from this study should be valuable in the development of other oriented metal-oxide NT electrodes for supercapacitor and other electrochemical applications.

Acknowledgment. This work was supported by the DOE/NREL Laboratory Directed Research and Development

DOI: 10.1021/nl102203s | *Nano Lett.* **2010,** *10,* 4099–4104

(LDRD) program under DOE Contract No. DE-AC36-08GO28308.

Supporting Information Available. XPS spectra of the Ti 2p and Ni 2p regions of the as-grown NT film and the Ni−Ti foil and NT film annealed at 600 °C, SAED pattern of the NT films annealed at 600 °C, cyclic voltammograms of the as-grown NT film and the Ni−Ti foil and NT film annealed at 600 °C, SEM images of the surface view of the NT films annealed at 700 °C, the scan rate dependence of the peak current density for NT films annealed at 600 °C, and the XRD patterns of NT films annealed from 400 to 700 °C. This material is available free of charge via the Internet at http://pubs.acs.org.

REFERENCES AND NOTES

(1) Zhu, K.; Neale, N. R.; Miedaner, A.; Frank, A. J. *Nano Lett.* **2007**, *7*, 69.
(2) Kuang, D.; Brillet, J.; Chen, P.; Takata, M.; Uchida, S.; Miura, H.; Sumioka, K.; Zakeeruddin, S. M.; Gratzel, M. *ACS Nano* **2008**, *2*, 1113.
(3) Mor, G. K.; Shankar, K.; Paulose, M.; Varghese, O. K.; Grimes, C. A. *Nano Lett.* **2006**, *6*, 215.
(4) Sun, W. T.; Yu, Y.; Pan, H. Y.; Gao, X. F.; Chen, Q.; Peng, L. M. *J. Am. Chem. Soc.* **2008**, *130*, 1124.
(5) Macak, J. M.; Tsuchiya, H.; Ghicov, A.; Schmuki, P. *Electrochem. Commun.* **2005**, *7*, 1133.
(6) Law, M.; Greene, L. E.; Johnson, J. C.; Saykally, R.; Yang, P. D. *Nat. Mater.* **2005**, *4*, 455.
(7) Baxter, J. B.; Aydil, E. S. *Appl. Phys. Lett.* **2005**, *86*, 3.
(8) Feng, X. J.; Shankar, K.; Varghese, O. K.; Paulose, M.; Latempa, T. J.; Grimes, C. A. *Nano Lett.* **2008**, *8*, 3781.
(9) Zhu, K.; Vinzant, T. B.; Neale, N. R.; Frank, A. J. *Nano Lett.* **2007**, *7*, 3739.
(10) Nah, Y. C.; Ghicov, A.; Kim, D.; Berger, S.; Schmuki, P. *J. Am. Chem. Soc.* **2008**, *130*, 16154.
(11) Ghicov, A.; Yamamoto, M.; Schmuki, P. *Angew. Chem., Int. Ed.* **2008**, *47*, 7934.
(12) Chan, C. K.; Peng, H. L.; Liu, G.; McIlwrath, K.; Zhang, X. F.; Huggins, R. A.; Cui, Y. *Nat. Nanotechnol.* **2008**, *3*, 31.
(13) Wang, D. W.; Fang, H. T.; Li, F.; Chen, Z. G.; Zhong, Q. S.; Lu, G. Q.; Cheng, H. M. *Adv. Funct. Mater.* **2008**, *18*, 3787.
(14) Wang, Q.; Wen, Z. H.; Li, J. H. *Adv. Funct. Mater.* **2006**, *16*, 2141.
(15) Ortiz, G. F.; Hanzu, I.; Djenizian, T.; Lavela, P.; Tirado, J. L.; Knauth, P. *Chem. Mater.* **2009**, *21*, 63.
(16) Han, K. S.; Lee, J. W.; Kang, Y. M.; Lee, J. Y.; Kang, J. K. *Small* **2008**, *4*, 1682.
(17) *Electrochemical Supercapacitors: Scientific Fundamentals and Technological Applications*; Conway, B. E., Ed.; Kluwer Academic/Plenum Publishers: New York, 1999.
(18) Conway, B. E.; Pell, W. G. *J. Solid State Electrochem.* **2003**, *7*, 637.
(19) Winter, M.; Brodd, R. J. *Chem. Rev.* **2004**, *104*, 4245.
(20) Miller, J. R.; Simon, P. *Science* **2008**, *321*, 651.
(21) Simon, P.; Gogotsi, Y. *Nat. Mater.* **2008**, *7*, 845.
(22) Stoller, M. D.; Park, S. J.; Zhu, Y. W.; An, J. H.; Ruoff, R. S. *Nano Lett.* **2008**, *8*, 3498.
(23) Zheng, J. P.; Jow, T. R. *J. Electrochem. Soc.* **1995**, *142*, L6.
(24) Zheng, J. P.; Cygan, P. J.; Jow, T. R. *J. Electrochem. Soc.* **1995**, *142*, 2699.
(25) Hu, C. C.; Chang, K. H.; Lin, M. C.; Wu, Y. T. *Nano Lett.* **2006**, *6*, 2690.
(26) Pang, S. C.; Anderson, M. A.; Chapman, T. W. *J. Electrochem. Soc.* **2000**, *147*, 444.
(27) Toupin, M.; Brousse, T.; Belanger, D. *Chem. Mater.* **2002**, *14*, 3946.
(28) Raymundo-Pinero, E.; Khomenko, V.; Frackowiak, E.; Beguin, F. *J. Electrochem. Soc.* **2005**, *152*, A229.
(29) Lin, C.; Ritter, J. A.; Popov, B. N. *J. Electrochem. Soc.* **1998**, *145*, 4097.
(30) Wei, T. Y.; Chen, C. H.; Chang, K. H.; Lu, S. Y.; Hu, C. C. *Chem. Mater.* **2009**, *21*, 3228.
(31) Liu, K. C.; Anderson, M. A. *J. Electrochem. Soc.* **1996**, *143*, 124.
(32) Srinivasan, V.; Weidner, J. W. *J. Electrochem. Soc.* **1997**, *144*, L210.
(33) Srinivasan, V.; Weidner, J. W. *J. Electrochem. Soc.* **2000**, *147*, 880.
(34) Nam, K. W.; Yoon, W. S.; Kim, K. B. *Electrochim. Acta* **2002**, *47*, 3201.
(35) Nam, K. W.; Kim, K. H.; Lee, E. S.; Yoon, W. S.; Yang, X. Q.; Kim, K. B. *J. Power Sources* **2008**, *182*, 642.
(36) Wang, Y. G.; Xia, Y. Y. *Electrochim. Acta* **2006**, *51*, 3223.
(37) Wu, M. S.; Huang, Y. A.; Yang, C. H.; Jow, H. H. *Int. J. Hydrogen Energy* **2007**, *32*, 4153.
(38) Lee, S. H.; Tracy, C. E.; Pitts, J. R. *Electrochem. Solid State Lett.* **2004**, *7*, A299.
(39) Zhao, D. D.; Xu, M. W.; Zhou, W. H.; Zhang, J.; Li, H. L. *Electrochim. Acta* **2008**, *53*, 2699.
(40) Wang, Y. G.; Zhang, X. G. *J. Electrochem. Soc.* **2005**, *152*, A671.
(41) Prasad, K. R.; Miura, N. *Appl. Phys. Lett.* **2004**, *85*, 4199.
(42) Zwilling, V.; Aucouturier, M.; Darque-Ceretti, E. *Electrochim. Acta* **1999**, *45*, 921.
(43) Zwilling, V.; Darque-Ceretti, E.; Boutry-Forveille, A.; David, D.; Perrin, M. Y.; Aucouturier, M. *Surf. Interface Anal.* **1999**, *27*, 629.
(44) Macak, J. M.; Tsuchiya, H.; Taveira, L.; Aldabergerova, S.; Schmuki, P. *Angew. Chem., Int. Ed.* **2005**, *44*, 7463.
(45) Varghese, O. K.; Gong, D. W.; Paulose, M.; Grimes, C. A.; Dickey, E. C. *J. Mater. Res.* **2003**, *18*, 156.
(46) Mor, G. K.; Prakasam, H. E.; Varghese, O. K.; Shankar, K.; Grimes, C. A. *Nano Lett.* **2007**, *7*, 2356.
(47) Mor, G. K.; Varghese, O. K.; Wilke, R. H. T.; Sharma, S.; Shankar, K.; Latempa, T. J.; Choi, K. S.; Grimes, C. A. *Nano Lett.* **2008**, *8*, 1906.
(48) Yasuda, K.; Schmuki, P. *Adv. Mater.* **2007**, *19*, 1757.
(49) Gong, D.; Grimes, C. A.; Varghese, O. K.; Hu, W. C.; Singh, R. S.; Chen, Z.; Dickey, E. C. *J. Mater. Res.* **2001**, *16*, 3331.
(50) Macak, J. M.; Tsuchiya, H.; Schmuki, P. *Angew. Chem., Int. Ed.* **2005**, *44*, 2100.
(51) Neale, N. R.; Kopidakis, N.; van de Lagemaat, J.; Gratzel, M.; Frank, A. J. *J. Phys. Chem. B* **2005**, *109*, 23183.

DOI: 10.1021/nl102203s | *Nano Lett.* **2010,** *10,* 4099–4104